JOURNAL OF MATERIALS SCIENCE 23 (1988) 1934–1942

Modelling of degradation of nickel-pigmented aluminium oxide photothermal collector coatings

A. SCHERER*, O. T. INAL, R. B. PETTIT‡
Department of Materials and Metallurgical Engineering, New Mexico Institute of Mining and Technology, Socorro, New Mexico 87801, USA and ‡Division 1824, Sandia National Laboratories, Albuquerque, New Mexico 87185, USA

Thermal degradation phenomena occurring in nickel-pigmented aluminium oxide coatings were investigated by combining detailed microstructural analysis with modelling of the optical properties. Scanning electron microscopy and Auger electron spectroscopy sputter profiling showed that the initial film consisted of a nickel-pigmented aluminium oxide layer close to the substrate. This layer supported a porous aluminium oxide layer that had a rough outer surface. While the solar absorptance degraded substantially (from 0.94 to 0.71) after heat treatment at 350° C for tens of hours, the aluminium oxide film morphology and thickness remained virtually unchanged and there was apparently no redistribution of nickel within the coating. Instead, the optical quality of the film degraded through oxidation of the nickel particles. These observations were supported by an optical model of the coating which produced the spectral reflectance properties measured both before and after the thermal ageing.

1. Introduction

Many of the most promising spectrally selective surfaces considered for use as solar collector coatings are composed of insulator–metal tandems [1]. Usually, the insulator constituent consists of a very thin metal oxide film (e.g. Al_2O_3, Cr_2O_3, MgO etc.), while the metal component consists of small particles (e.g. chromium, nickel, platinum etc.) that are typically embedded in the insulator matrix. To minimize the first-surface reflectance losses and provide a high solar absorptance, these metal–metal-oxide layers possess a refractive index gradient allowing a smooth increase from the refractive index of air to that of the substrate [2, 3]. However, in the infrared wavelength range where large reflectance values are desired to minimize the amount of thermal radiation [4, 5], these coatings are highly transparent to the incident radiation so that the reflectance is dominated by the metallic substrate.

It has become clear that several effects, such as wavefront discrimination and dispersions of metal particles in a dielectric matrix, usually contribute to the optical quality of selective solar absorbers [6]. The effects of these contributions can be explained by fundamental optical relationships, once detailed information on the structure of the coatings and the dielectric properties of the constituents are obtained [7]. Conversely, the resulting optical properties as functions of wavelength can be a very valuable means of providing further insight into the internal structures of such layers [8].

The combination of a high solar absorptance with a low thermal emittance has previously been reported for thin films of nickel-pigmented aluminium oxide [4, 5, 9]. These coatings consist of a porous aluminium oxide matrix containing microcrystalline nickel particles deposited in the pores [5]. The size of the nickel particles is determined by the pore size in the aluminium oxide matrix. While the optical properties and structure of as-deposited nickel-pigmented aluminium oxide have previously been reported [5, 9], the degradation phenomena of this coating during thermal heat treatment, humidity/temperature, or outdoor exposure have not been investigated.

Evaluation of changes in the optical properties of such structurally complex layers that occur during accelerated testing can be used to elucidate the mechanism of degradation [10]. The intent of the present study is to characterize, through microstructural analysis and optical modelling, the thermal degradation phenomena occurring in nickel-pigmented aluminium oxide solar collector coatings. In addition, a generalized multilayer coating model consistent with microstructural analyses is used to account for surface roughness and the effect of nickel dispersed in the anodic oxide layer. Finally, this study also investigated the influence of other environmental exposures, such as humidity and outdoor exposure, on this selective absorber system. If the degradation mechanism occurring in these photothermal collector surfaces can be determined, then the long-term durability of the coatings can be estimated with reasonable accuracy through extrapolation of accelerated test results. In

**Present address*: Bell Communications Research, Red Bank, New Jersey 08801, USA.

0022–2461/88 $03.00 + .12

addition, the structure of coatings previously optimized for short-term thermal stability [4] can be identified.

2. Experimental procedure

2.1. Overview of this study

The generation of degradation information on a selective absorber coating requires the performance of systematic heat treatments. Structural and optical changes are recorded after the heat treatment, and detailed analysis is undertaken to elucidate significant changes in the coating structure and composition. In this investigation, the optical data gathered are primarily the solar averaged absorptance and thermal emittance (at 80° C), which provide measures of the optical quality of the spectrally selective surfaces. Spectral reflectance properties, which are necessary for detailed optical modelling, were also obtained on samples showing significant changes in these properties. Furthermore, Auger depth profiles were generated on samples of particular interest to verify the existence and shapes of compositional gradients within the films.

This information was then used to develop a structural model of the as-deposited films and to determine how this structure changed with thermal ageing. The structural model was designed to reproduce the measured spectral reflectance properties of as-deposited films while being consistent with measured coating structural data. To verify the model, the measured changes in the spectral reflectance properties with thermal ageing were compared with the results predicted by the model.

2.2. Preparation of the coatings

Commercial-grade aluminium (1100-0 Aluminum Association) substrates were first chemically polished at 90 to 95° C for 30 to 60 sec in a solution consisting of 20 vol % nitric, 25 vol % sulphuric and 55 vol % phosphoric acid with the addition of 1.8 gl^{-1} ferrous sulphate. These 5 cm × 5 cm aluminium substrates were anodized in 3.25 M phosphoric acid at a potential of 12.5 V (d.c.) for 20 min. These are the optimum conditions for the production of films with a high porosity and with sufficient structural integrity [11]. Following this treatment the coatings were neutralized for 2 h in a 20 gl^{-1} sodium bicarbonate solution before being pigmented, using the following bath composition and plating conditions [12]:

Nickel acetate	35 gl^{-1}
Diethanolamine	17.5 $ml\,l^{-1}$
Boric acid	45 gl^{-1}
Voltage	14 V
Temperature	25° C
Time	8 min

This process typically yielded as-plated solar absorptance values of 0.94 and 80° C thermal emittance values of 0.20.

2.3. Heat treatments

Heat treatments were performed in muffle furnaces operating in the range of 150 to 350° C with temperature control and uniformity of better than ± 5° C. Anodized and nickel-pigmented plates were exposed to heat treatments at 350, 250, 205 and 150° C. One of these plates provided samples for microstructural analysis at the various heat-treatment temperatures, whereas the others were evaluated optically. When a series of coatings was particularly degraded, an intact sample of that coating was removed and its spectral reflectance against wavelength behaviour measured. Heat treatments were terminated either when the optical properties had stabilized or when the samples were too degraded to provide any useful information.

Temperature/humidity and outdoor exposure tests were conducted to obtain both optical data as well as microstructural information after ageing in different environments. Humidity tests were performed at 150° C in water-vapour saturated air. Outdoor exposures were conducted in a collector designed to reproduce stagnation conditions. This collector was oriented towards the south at a 30° inclination, with a 5 cm air gap between the Plexiglas cover plate and the samples. Typical daytime sample temperatures ranged from 60 to 100° C depending upon weather conditions.

2.4. Electron microscopy

A Hitachi Perkin–Elmer HHS-2R scanning electron microscope (SEM) was used to determine approximate thicknesses of the coatings. The surface morphologies of the sample were also established both before and after heat treatment or other testing conditions. An RCA EMU-3G transmission electron microscope (TEM) was used to analyse the anodically formed aluminium oxide layers prior to pigmentation, which were detached by amalgamation [11]. This instrument was also utilized to obtain reflection electron diffraction (RED) patterns [13] of as-plated and heat-treated samples.

2.5. Optical property measurements

Solar absorptance values for the coatings were measured using a Gier–Dunkle solar reflectometer, Model MS-251. The performance of this instrument has been reported elsewhere [14]. The solar absorptance values should be accurate to about ± 0.03 absorptance units. The normal, total emittance values of the coatings were measured with a Devices and Services emissometer operating at 80° C and should be accurate to about ± 0.04 emittance units [14]. Spectral reflectance properties over the wavelength range 300 to 2400 nm were measured with a Beckman model 5270 spectrophotometer with an integrating sphere accessory and are accurate to ± 0.01 reflectance units.

3. Results

3.1. Degradation of the optical properties

The solar absorptance and 80° C emittance properties for nickel-pigmented aluminium oxide are shown in Figs 1a and b, respectively. The solar absorptance of the nickel-pigmented aluminium oxide coatings was observed to be sensitive to thermal exposure and to degrade substantially during heat treatments at 350° C for tens of hours as well as at 205° C when exposed for 2258 h. The emittance generally decreased with time

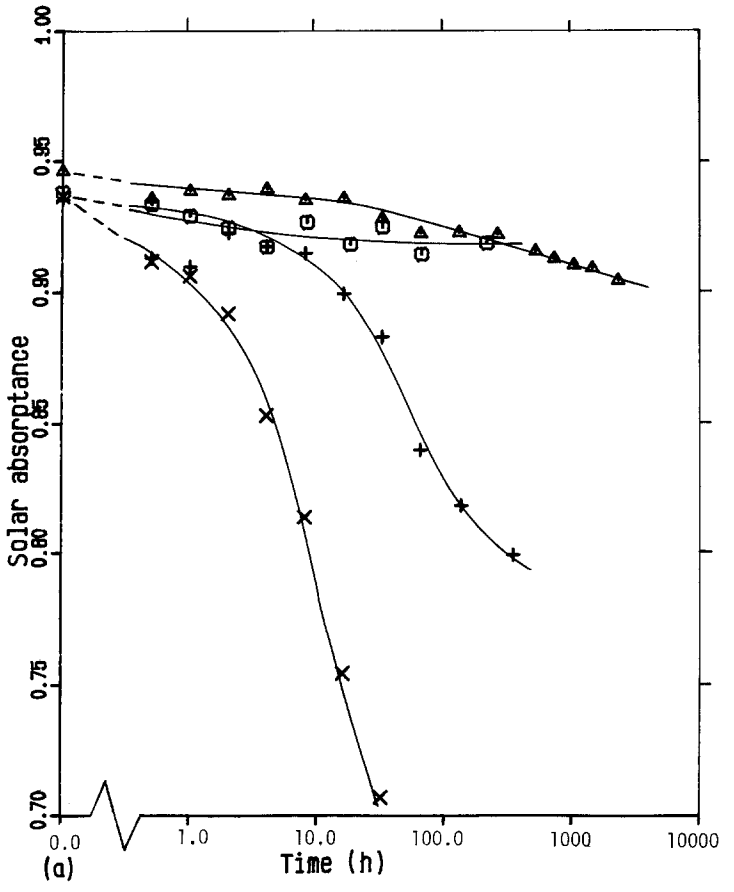

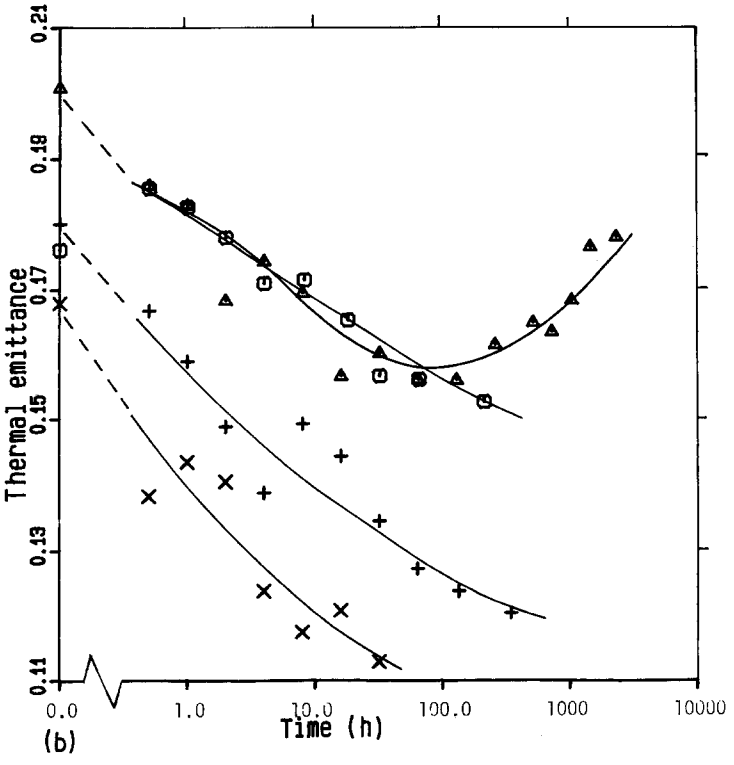

Figure 1 (a) Solar absorptance of nickel-pigmented aluminium oxide as a function of heat-treatment time at several temperatures: (□) 150, (△) 205, (+) 250, (x) 350° C. (b) Thermal emittance against exposure time for several temperatures: (□) 150, (△) 205, (+) 250, (x) 350° C.

during the heat treatments. Humidity at 150° C was found to have only a slight influence on the solar absorptance as compared to heat treatments in muffle furnaces at the same temperature. Outdoor exposure for 156 days degraded the solar absorptance from 0.94 to 0.92 and the 80° C emittance from 0.20 to 0.13.

Spectral reflectance properties are shown in Fig. 2 for both as-deposited and aged coatings. For an as-deposited sample, the reflectance is essentially constant at ≈ 0.03 through the visible region. It then rapidly increases to values above 0.10 near 1200 nm and finally decreases again at higher wavelengths. The oscillations in the reflectance in the near infrared appear to be the result of interference effects. With thermal ageing, two changes in the curves are evident. First, the maximum reflectance value near 1200 nm increases as the heat-treatment temperature or time is increased. Secondly, the position of this maximum shifts slightly to lower wavelengths. The increase in

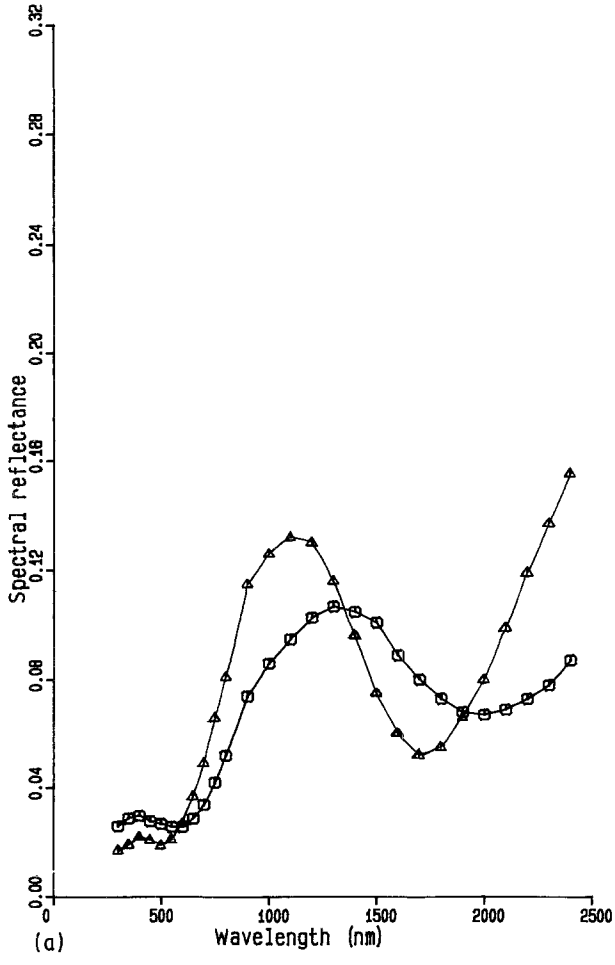

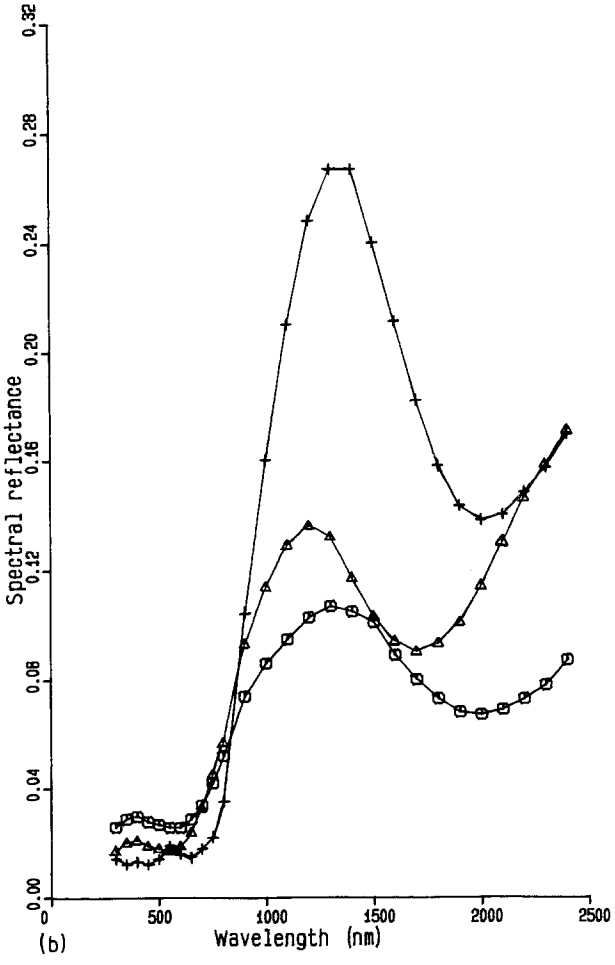

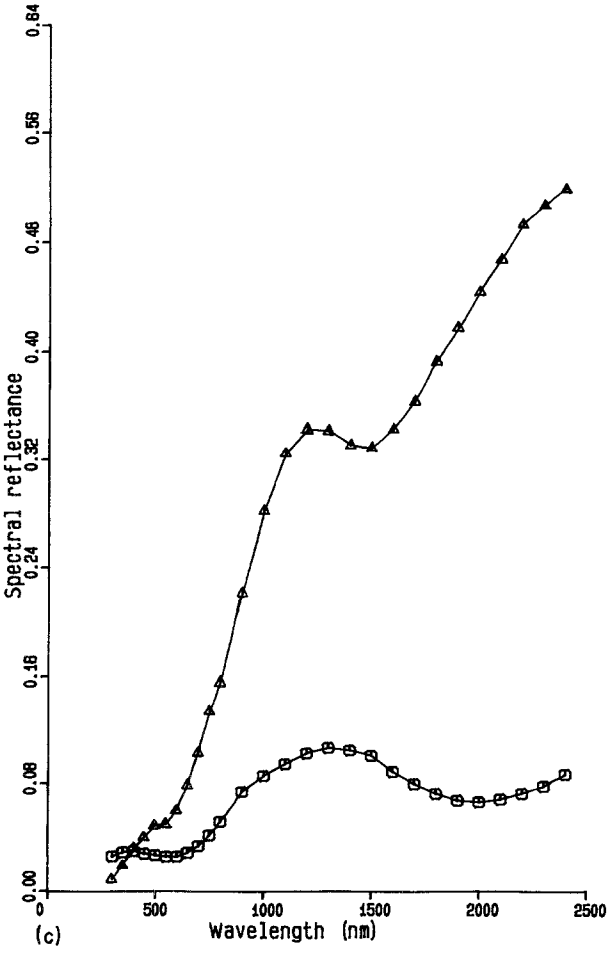

Figure 2 (a) Measured spectral reflectance properties for (□) as-coated nickel pigmented aluminium oxide compared to (△) a coating heated to 150° C for 18 h. (b) Measured spectral reflectance properties after heat treatment to 205° C for (△) 128 and (+) 2258 h; (□) as-coated. (c) Measured spectral reflectance properties (△) after heat treatment to 350° C for 18 h; (□) as-coated.

reflectance values with heat treatment result in the observed decrease in the solar absorptance.

3.2. Microstructural analysis

Previous microstructural analysis on anodized aluminium coatings have shown a strong dependence of the coating microstructure and porosity on the anodizing voltage as well as the pH of the electrolyte [15]. Coatings 0.8 μm thick were produced using anodization parameters from a previous study that optimized the pore volume fraction (Fig. 3a). The porosity was determined to be approximately 30% from TEM analysis of detached oxide layers (Fig. 3b) [11].

During the pigmentation step, the aluminium oxide layer did not change in morphology, although the appearance of the film turned jet-black. An SEM micrograph of an as-plated coating is shown in Fig. 4a, while micrographs after heat treatments at 250° C are shown in Figs 4b to d. The film morphology and overall thickness were observed to remain unaffected by such exposure. No change in the film structure could be detected from SEM micrographs even after severe heat treatment at 350° C. Degradation,

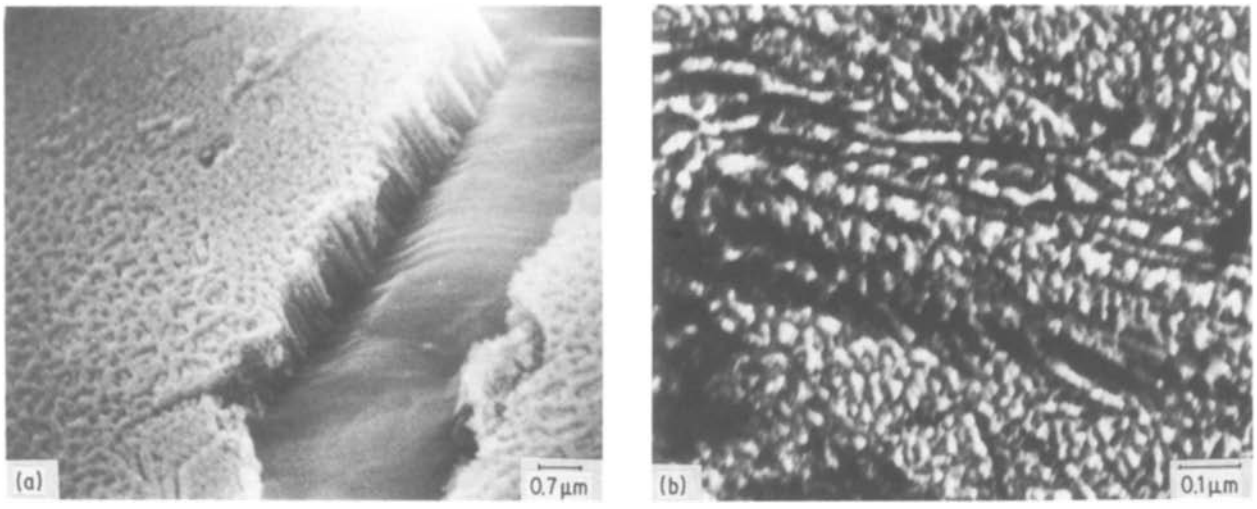

Figure 3 (a) SEM micrograph of an unpigmented aluminium oxide film produced under optimal anodizing conditions as discussed in the text. (b) TEM micrograph of an aluminium oxide film with the same anodization conditions.

therefore, must be related to a change in the structure within these films and not to any change in the surface roughness or thickness of the aluminium oxide. Since anodic aluminium oxide coatings produced at low voltages are generally amorphous, RED did not provide any insight into the surface oxide structure. However, X-ray diffraction analyses of these coatings revealed a substantial decrease in the metallic nickel peak intensity during thermal exposure, which can be attributed to oxidation of the nickel particles.

Auger electron spectroscopy (AES) sputter profiles reveal a substantial nickel signal only close to the substrate aluminium (Figs 5a to c). Thus the nickel is deposited in the bottom of the pores in the aluminium oxide. This explains why the RED patterns from the surface did not show the presence of nickel in the coating. If the substrate–coating interface is defined by the point where the nickel signal falls to half of its peak value, the time to sputter to this interface is unchanged during thermal exposure. Therefore, it

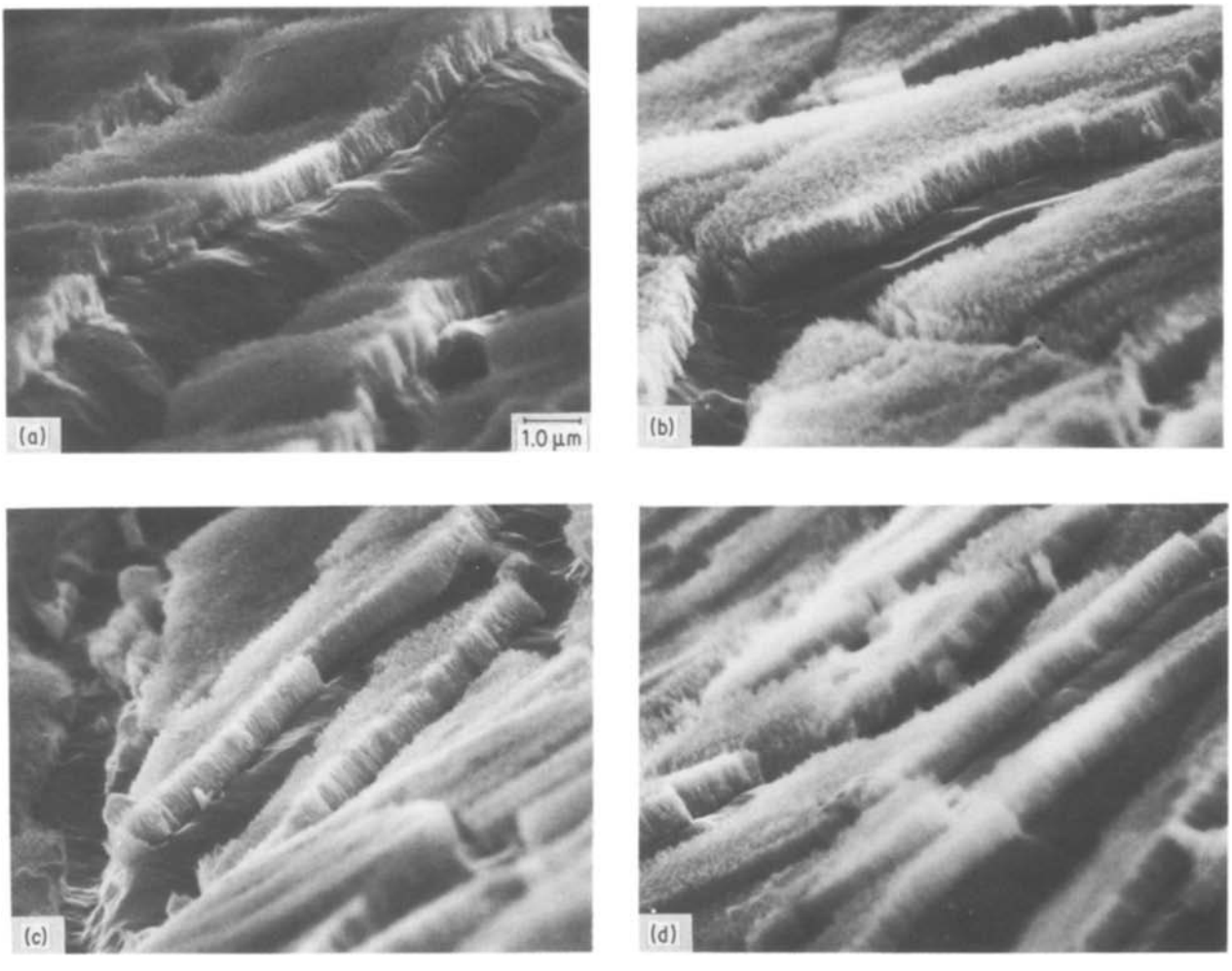

Figure 4 SEM micrograph of pigmented oxide films (a) as-deposited, (b) after 4 h at 250° C, (c) after 100 h at 250° C, (d) after 32 h at 350° C.

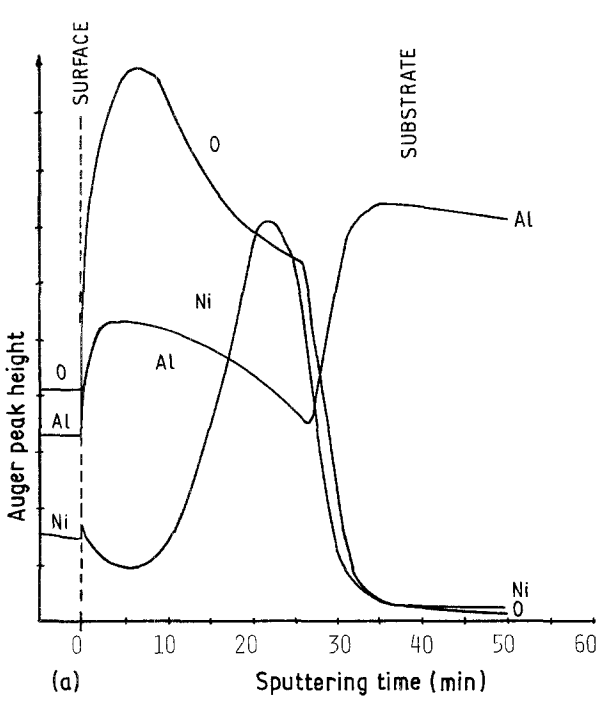

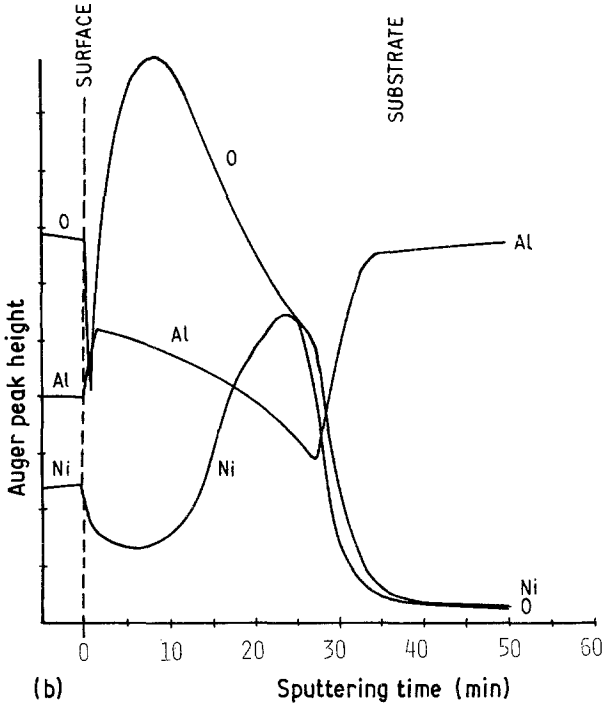

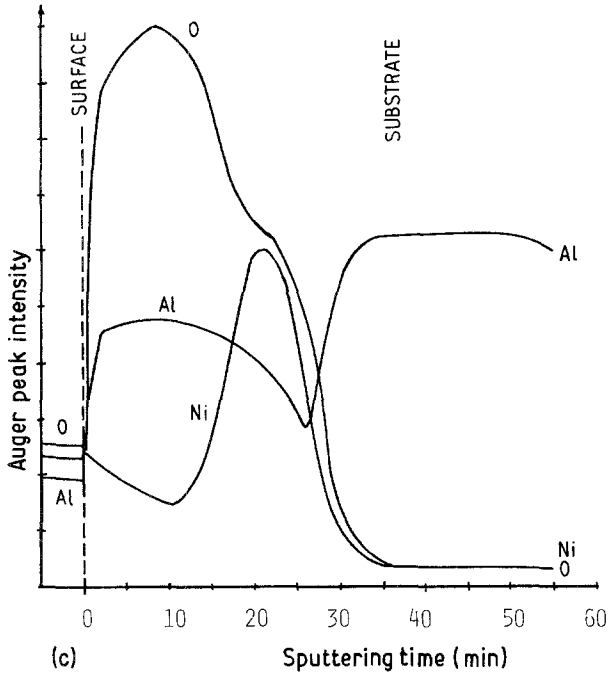

Figure 5 AES sputter profiles of pigmented coatings (a) as-deposited, (b) after heat treatment to 205° C for 128 h (c) after heat treatment to 350° C for 32 h.

appears that the film thickness is not substantially changed during heat treatment, in agreement with the SEM results. Since the nickel signal decreases simultaneously with the oxide signal at the film–substrate interface (after 30 min of sputtering), the maximum volume fraction of nickel is believed to be present at the substrate [16]. Although a nickel signal is observed at the surface of the film, it is believed that the nickel is primarily deposited in the bottom of the pores in the aluminium oxide. This nickel signal results from the fact that the pores above the nickel are open, thus allowing a nickel signal to be detected from the surface. Although volume fractions of nickel and aluminium oxide cannot directly be obtained from the AES data, the maximum nickel content in the oxide can be approximated by the porosity of the anodic aluminium oxide film, which is 30%. Essentially no change in the nickel profile was detected after heat treatment, which would indicate no redistribution of the nickel in the coating. However, after the heat treatment, a slight increase in the oxygen signal relative to the nickel signal can be observed which indicates that some oxidation of the nickel has occurred.

4. Optical modelling

4.1. Calculation of the optical properties

Computer modelling was done using an iterative program for the calculation of complex Fresnel coefficients at normal incidence of a multilayer stack. The coating was subdivided into a large number of layers, each of which contained uniform but different volume fractions of particles dispersed in a matrix. Although a very large number of slices could be modelled, it was found that there was no advantage in using over 50 slices in each sublayer. The Maxwell–Garnett effective medium theory [7] was used to determine the composite complex index of refraction of individual slices. Optical property data for each layer were provided by a subroutine which generated complex refractive index values using dielectric constants calculated from an effective medium theory. These slices were then stacked, according to Rouard's method [17], on top of the substrate. Reflectance against wavelength data generated by the model were then plotted and compared with the experimental data obtained from both as-plated and degraded samples to evaluate the parameters in the model.

4.2. Optical property data

The complex index of refraction ($\tilde{n} = n - ik$) of aluminium and nickel are tabulated in the AIP handbook [18] as well as the manuscript by Ordal *et al.* [19]. These data were combined, and the refractive index against wavelength behaviour compiled as shown in

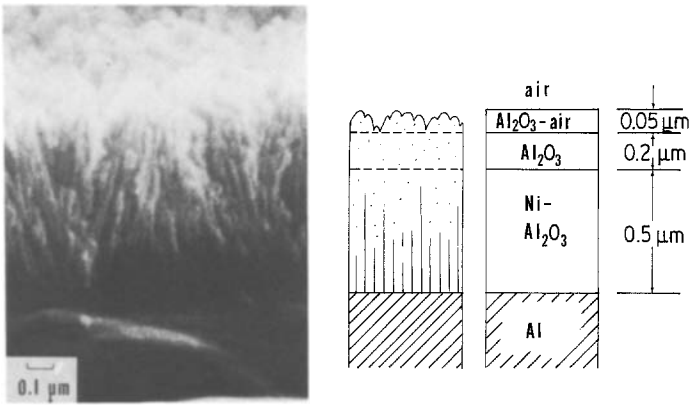

Figure 6 Schematic diagram of structural model of nickel-pigmented aluminium oxide compared to an SEM micrograph of a fractured coating.

Table I. For anodically formed aluminium oxide, the refractive index can be assumed to be a constant throughout the spectrum of interest and was set equal to 1.66, in agreement with previous optical models of anodic oxide deposits on aluminium [5]. The index of refraction of the nickel oxide that formed in the coating during thermal ageing was assumed to compare closely to the value used for the aluminium oxide of 1.66.

4.3. Coating model

When nickel is electrodeposited into an aluminium oxide film, spectral selectivity arises both from the resultant refractive index gradient and the high absorptance of small nickel particles [20]. These effects have in the past been thoroughly studied for as-plated, pigmented, anodic oxide deposits, and the film geometry of these layers has been described using several effective medium theories [5, 9, 21, 22]. However, no attempt has been made to analyse the optical degradation of such films during thermal exposure.

Based on the microstructural analysis, the coating could be naturally divided into three layers. The layer closest to the substrate was modelled as a nickel-

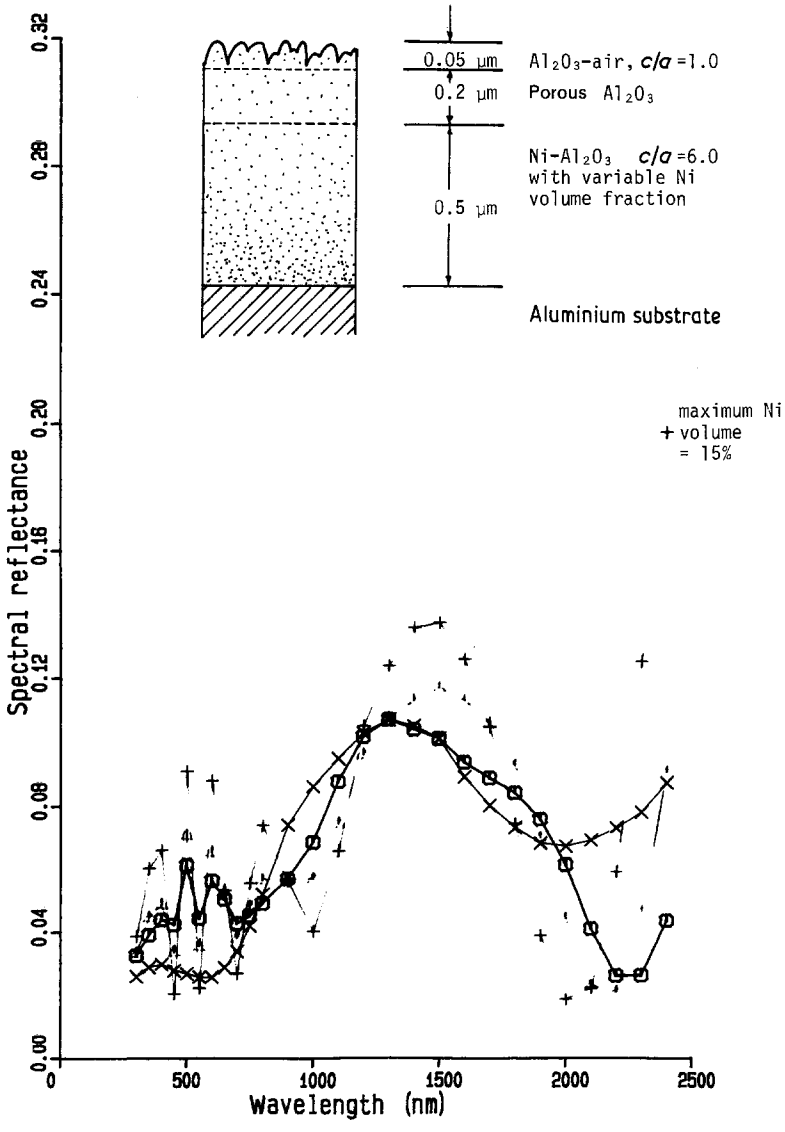

Figure 7 Effect of a change in the maximum nickel volume fraction (at the substrate interface) on the calculated spectral reflectance properties. Maximum nickel volume (+) 15%, (△) 20%, (□) 25%; (x) measured as-plated.

TABLE I Optical properties of nickel and aluminium used in the reflectance calculations

Wavelength (nm)	Aluminium		Nickel	
	n	*k*	*n*	*k*
300	0.25	3.50	1.60	2.25
350	0.30	4.30	1.70	2.50
400	0.40	5.00	1.73	2.75
450	0.50	5.75	1.79	3.00
500	0.70	6.25	1.82	3.25
550	0.90	6.90	1.90	3.60
600	1.25	7.40	1.95	4.00
650	1.75	7.75	2.00	4.25
700	2.27	7.95	2.06	4.50
750	2.63	8.13	2.15	4.75
800	2.75	8.30	2.25	5.00
900	2.63	9.00	2.40	5.25
1000	2.13	10.6	2.50	5.65
1100	1.60	12.1	2.63	6.05
1200	1.27	13.2	2.69	6.20
1300	1.23	14.1	2.90	6.80
1400	1.25	15.0	3.00	7.25
1500	1.40	15.6	3.10	7.50
1600	1.50	16.6	3.12	7.90
1700	1.65	17.8	3.20	8.25
1800	1.75	18.8	3.30	8.60
1900	1.90	19.8	3.45	8.90
2000	2.05	21.0	3.55	9.25
2100	2.13	21.7	3.62	9.50
2200	2.25	22.7	3.70	9.80
2300	2.30	23.7	3.80	10.15
2400	2.35	24.6	3.85	10.40

pigmented layer containing a linear nickel volume-fraction gradient varying from a maximum value at the substrate–oxide interface to 0% at its outer boundary. The porosity of the initial anodic oxide coating determined by TEM provided an upper boundary of the maximum nickel volume fraction in this layer (30%). The cylindrical pore shape means that the resulting nickel particles have a high length (c) to width (a) ratio [23]. In calculating the effective dielectric constant for this layer, the long axis of these nickel particles was oriented perpendicular to the substrate and thus parallel to the incident radiation. The pigmented aluminium oxide layer supports a porous but unpigmented aluminium oxide intermediate layer. Finally, the coating surface roughness was taken into account by a third layer which was modelled to contain a linear volume fraction of aluminium oxide particles in an air matrix. The total coating thickness was measured as approximately 0.8 μm, with a rough surface layer of approximately 0.05 μm.

The following variables were incorporated into the three-layer structural model (Fig. 6):

1. Nickel–alumina thickness 0.5 μm
   Maximum volume fraction of nickel 0.30
   Volume fraction gradient Linear
   c/a ratio of nickel particles 6
2. Thickness of pure oxide 0.2 μm

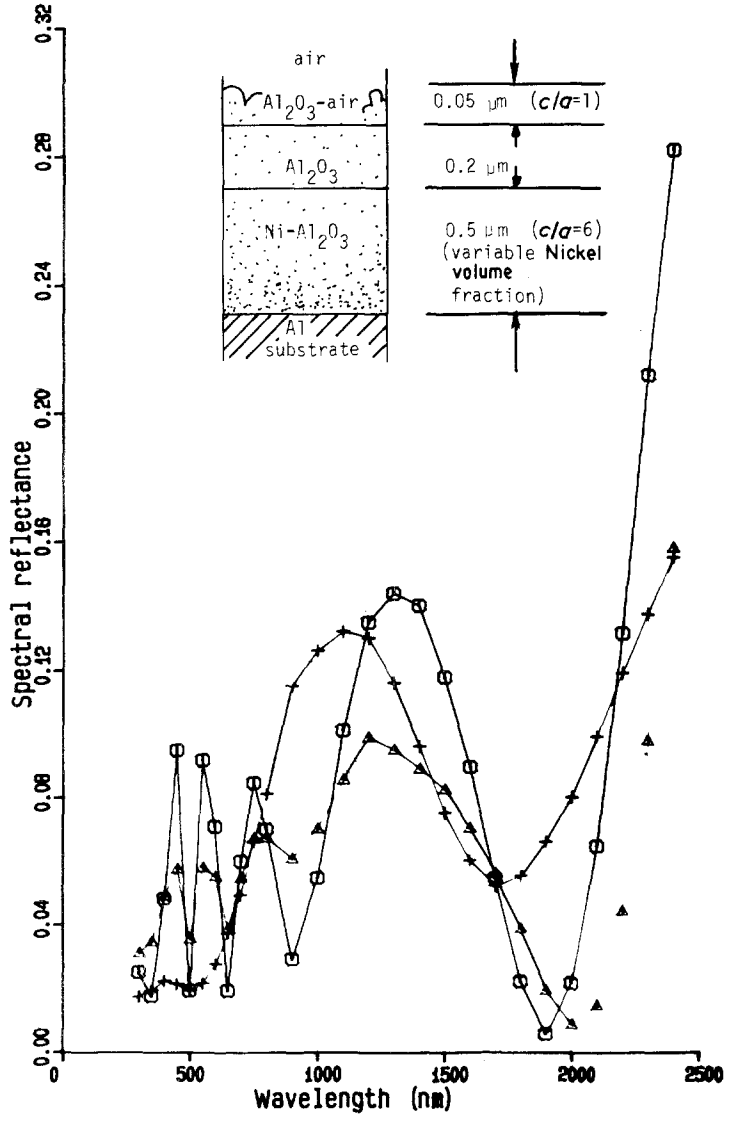

Figure 8 Model prediction of the combined effect of a decrease in the pigmented oxide thickness with a decrease in the maximum nickel volume fraction on the calculated spectral reflectance properties. (□) Ni–Al_2O_3 = 0.45 μm, f_{Ni} = 15%; (△) Ni–Al_2O_3 = 0.50 μm, f_{Ni} = 20%; (+) measured after 18 h at 150° C.

3.	Thickness of surface roughness	0.05 μm
	c/a ratio of alumina particles	1.0

Calculations showing the effect of varying the maximum volume fraction of nickel at the substrate interface are shown in Fig. 7. If the maximum volume fraction of nickel in the pigmented oxide layer is decreased, the interference peak in the spectral reflectance curve becomes more pronounced (Fig. 7). This behaviour resembles the low-temperature (150 to 205° C) exposure behaviour shown in Figs 2a and b. Additional calculations show that a decrease in the pigmented oxide layer thickness causes a shift of that peak to shorter wavelengths. If these two effects are combined, the measured reflectance behaviour with ageing shown in Fig. 2a can be reproduced (Fig. 8).

Thermal exposure of nickel-pigmented aluminium oxide can therefore be described by an increase of the unpigmented oxide layer thickness at the expense of the nickel-pigmented aluminium oxide layer so that the total film thickness remains constant. This trend should continue until a virtually transparent coating is obtained after severe heat treatments.

5. Discussion and conclusions

Several attempts have been made in the past to model pigmented aluminium oxide films [5, 9, 20, 21]. Films produced by sulphuric acid anodizing followed by electrolytic pigmentation were described as a 0.35 μm thick stack of porous alumina containing metal particles close to the substrate [9]. Similarly, Andersson *et al.* [5] reported deposits produced in phosphoric acid to consist of approximately 0.7 μm thick oxide layers with nickel dispersed at the bottom of the pores.

These observations match the structural information obtained in this study, where 0.8 μm thick structures were observed to fit the measured reflectance response of the as-plated deposits. A three-layer stack, consisting of pigmented oxide with a linear nickel volume fraction gradient, pure anodic oxide, and a rough oxide–air interface, was found to reproduce the as-coated reflectance behaviour measured on these coatings. Heat treatment of this coating was found not to influence the thickness or roughness of the oxide, and degradation proceeded through oxidation of the nickel with no significant redistribution of this dispersed metal. The agreement of measured and calculated reflectance properties supports this observation.

Acknowledgements

The authors are indebted to Mr J. L. Rife of Sandia National Laboratories, who obtained the Auger electron spectroscopy sputter profiles for this study. This research was funded in part by the US Department of Energy, under Division of Materials Science Contract No. DE-ER-78-04-4266, and is gratefully acknowledged. Portions of this work performed at Sandia National Laboratories were also supported by the US Department of Energy, under Contract No. DE-AC04-76-DP00789.

References

1. H. G. CRAIGHEAD, R. BARTYNSKI, R. A. BUHRMAN, L. WOJCIK and H. J. SIEVIRS, *Sol. Energy Mater.* **1** (1979) 105.
2. R. A. BUHRMAN and H. G. CRAIGHEAD, in "Solar Materials Science", edited by L. E. Murr (Academic, New York 1980) p. 294.
3. A. B. MEINEL and M. P. MEINEL, "Applied Solar Energy – An Introduction" (Addison-Wesley, Reading, Massachusetts, 1976) p. 303.
4. O. T. INAL and A. SCHERER, *J. Mater. Sci.* **21** (1986) 729.
5. A. ANDERSSON, O. HUNDERI and C. G. GRANQVIST, *J. Appl. Phys.* **51** (1980) 754.
6. G. ZERLAUT, in "Critical Materials Problems in Energy Production", edited by C. Stein (Academic, New York, 1976) p. 889.
7. H. G. CRAIGHEAD and R. A. BUHRMAN, *J. Vac. Sci. Technol.* **15** (1978) 269.
8. D. E. ASPNES, *Thin Solid Films* **89** (1982) 249.
9. R. D. PATEL, M. G. TAKWALE, V. K. NAGAR and V. G. BHIDE, *ibid.* **115** (1984) 169.
10. L. W. MASTERS, J. F. SEILER, E. J. EMBREE and W. E. ROBERTS, "Solar Energy Systems – Standards for Absorber Materials", US DOC NBSIR 81-2232 (1981).
11. A. SCHERER and O. T. INAL, *Thin Solid Films* **101** (1983) 311.
12. K. WADA, T. HATANO and K. UCHIDA, *J. Appl. Electrochem.* **9** (1979) 445.
13. A. SCHERER and O. T. INAL, *Thin Solid Films* **19** (1984) 413.
14. G. N. SWEAT, R. B. PETTIT and M. B. CHAMBERLAIN, *Sol. Energy Mater.* **10** (1984) 251.
15. S. TAJIMA, in "Advances in Corrosion Science and Technology, Vol. I (1970) pp. 229–362.
16. A. K. GRAHAM, "Electroplating Engineering Handbook" (Reinhold, New York, 1955) p. 457.
17. O. S. HEAVENS, "Optical Properties of Thin Solid Films" (Dover, New York, 1965) p. 141.
18. D. E. GRAY (ed.), "American Institute of Physics Handbook", 3rd Edn, (McGraw-Hill, New York, 1972) pp. 6-124 to 6-155.
19. M. A. ORDALL, L. L. LONG, R. J. BELL, S. E. BELL, R. R. BELL, R. W. ALEXANDER Jr and C. A. WARD, *Appl. Opt.* **22** (1983) 1099.
20. C. G. GRANQVIST and O. HUNDERI, *Appl. Phys. Lett.* **32** (1978) 798.
21. D. G. W. GOAD and M. MOSKOVITS, *J. Appl. Phys.* **49** (1978) 2929.
22. R. CHANG and W. F. HALL, *Thin Solid Films* **46** (1977) L5.
23. L. SANDERA, *Aluminium* **49** (1973) 533.

Received 3 November
and accepted 28 January 1987